

1 Chemical Characterization of Submicron Aerosol and Particle Growth
2 Events at a National Background Site (3295 m a.s.l.) on the Tibetan
3 Plateau

4
5 W. Du^{1,2}, Y. L. Sun^{1,*}, Y. S. Xu³, Q. Jiang¹, Q. Q. Wang¹, W. Yang³, F. Wang³, Z. P.
6 Bai³, X. D. Zhao⁴, and Y. C. Yang²

7
8 ¹*State Key Laboratory of Atmospheric Boundary Layer Physics and Atmospheric Chemistry,*
9 *Institute of Atmospheric Physics, Chinese Academy of Sciences, Beijing 100029, China*

10 ²*Department of Resources and Environment, Air Environmental Modeling and Pollution*
11 *Controlling Key Laboratory of Sichuan Higher Education Institutes, Chengdu University of*
12 *Information Technology, Chengdu 610225, China*

13 ³*Chinese Research Academy of Environmental Sciences, Beijing 100012, China*

14 ⁴*National Station for Background Atmospheric Monitoring, Menyuan, Qinghai 810000,*
15 *China*

16
17
18 *Correspondence to: Y. L. Sun (sunyele@mail.iap.ac.cn)

19 **Abstract**

20 Atmospheric aerosols exert highly uncertain impacts on radiative forcing and also
21 have detrimental effects on human health. While aerosol particles are widely
22 characterized in megacities in China, aerosol composition, sources and particle
23 growth in rural areas in the Tibetan Plateau remain less understood. Here we present
24 the results from an autumn study that was conducted from 5 September to 15 October
25 2013 at a national background monitoring station (3295 m a.s.l.) in the Tibetan
26 Plateau. The submicron aerosol composition and particle number size distributions
27 were measured in situ with an Aerodyne Aerosol Chemical Speciation Monitor
28 (ACSM) and a Scanning Mobility Particle Sizer (SMPS). The average mass
29 concentration of submicron aerosol (PM_{10}) is $11.4 \mu\text{g m}^{-3}$ (range: $1.0 - 78.4 \mu\text{g m}^{-3}$) for
30 the entire study, which is much lower than those observed at urban and rural sites in
31 eastern China. Organics dominated PM_{10} on average accounting for 43%, followed by
32 sulfate (28%) and ammonium (11%). Positive matrix factorization analysis of ACSM
33 organic aerosol (OA) mass spectra identified an oxygenated OA (OOA) and a biomass
34 burning OA (BBOA). The OOA dominated OA composition accounting for 85% on
35 average, 17% of which was inferred from aged BBOA. The BBOA contributed a
36 considerable fraction of OA (15%) due to the burning of cow dung and straws in
37 September. New particle formation and growth events were frequently observed (80%
38 of time) throughout the study. The average particle growth rate is 2.0 nm hr^{-1} (range:
39 $0.8 - 3.2 \text{ nm hr}^{-1}$). By linking the evolution of particle number size distribution to
40 aerosol composition, we found an elevated contribution of organics during particle
41 growth periods and also a positive relationship between the growth rate and the
42 fraction of OOA in OA, which potentially indicates an important role of organics in
43 particle growth in the Tibetan Plateau.

44

45 **1 Introduction**

46 High concentration of atmosphere aerosol associated with the rapid economic
47 growth, urbanization and industrialization has become a major environmental concern
48 in China. Aerosol particles especially fine particles ($PM_{2.5}$) have large impacts on
49 human health, natural ecosystem, weather and climate, radiative balance and the
50 self-purification capacity of troposphere (Jacobson, 2001; Tie and Cao, 2009). As a
51 result, a large number of studies have been conducted to investigate the sources,
52 chemical and physical properties, and evolution processes of aerosol particles at urban
53 and rural sites in China during the last decade (Cao et al., 2007; Wu et al., 2007; He et
54 al., 2011; Gong et al., 2012; Huang et al., 2012; Huang et al., 2013; Sun et al., 2013;
55 Jiang et al., 2015). The results showed that fine particles are mainly composed of
56 organics, sulfate, nitrate, ammonium, mineral dust, and black carbon. The sources of
57 organic aerosol (OA) were also characterized and various OA factors from distinct
58 sources were identified including primary OA (POA), e.g., hydrocarbon-like OA
59 (HOA), cooking OA (COA), biomass burning OA (BBOA) and coal combustion OA
60 (CCOA), and secondary OA (SOA), e.g., semi-volatile oxygenated OA (SV-OOA)
61 and low volatility OOA (LV-OOA) (Huang et al., 2010; Sun et al., 2010; He et al.,
62 2011; Huang et al., 2011; Xu et al., 2014a; Sun et al., 2014). While previous studies
63 significantly improve our understanding on the sources and chemical properties of
64 aerosol particles, they were mainly conducted in developed areas in China, including
65 Beijing-Tianjin-Hebei, Pearl River Delta and Yangtze River Delta.

66 The Tibetan Plateau (~ 2,000,000 square kilometers) is the highest plateau in the
67 world with an average altitude of over 4000 meters above sea level. The Tibetan
68 Plateau is an ideal location for charactering rural and regional background aerosol due
69 to minor influences of anthropogenic activities. However, chemical characterization
70 of aerosol particles in the Tibetan Plateau is rather limited, and therefore their sources,
71 properties, and evolution processes are poorly known. Cong et al. (2015) reported the
72 seasonal variations of various aerosol components including carbonaceous species
73 and water-soluble ionic species on the south edge of the Tibetan Plateau. Sulfate was
74 found to dominate the total ionic mass (25%) followed by nitrate. In addition, most

75 aerosol species showed pronounced season variations in the pre-monsoon period due
76 to biomass burning impacts from India and Nepal. Zhao et al. (2013) also
77 characterized the chemical composition and sources of total suspended particulate
78 (TSP) at Lulang on the southeastern TP based on one year measurement. Similar
79 seasonal variations with higher concentrations during pre-monsoon were observed.
80 The back trajectory analysis showed evident transport of air pollutants from south
81 Asia to the TP. The analysis of size-segregated aerosol samples collected at a remote
82 site in the inland Tibetan Plateau during 2012 further confirmed the high
83 concentrations of organic carbon (OC) and elemental carbon (EC) during the
84 pre-monsoon period (Wan et al., 2015), although their concentrations in PM₁ (2.38
85 and 0.08 $\mu\text{g m}^{-3}$, respectively) were much lower than those reported in eastern China.
86 Most studies above were conducted in the southeastern Tibetan Plateau.
87 Comparatively, aerosol particles showed quite different behavior in the northeastern
88 Tibetan Plateau. Li et al. (2013) investigated the sources and chemical composition of
89 fine particles collected at a remote site (Qinghai Lake) in the summer of 2010 in the
90 Tibetan Plateau. The average PM_{2.5} concentration was $22 \pm 13 \mu\text{g m}^{-3}$ with sulfate and
91 carbonaceous aerosol being the two major species. Xu et al. (2014b) conducted a
92 year-long measurement of PM_{2.5} composition at the Qilian Shan Station, The annual
93 average concentration of PM_{2.5} was $9.5 \pm 5.4 \mu\text{g m}^{-3}$ with water-soluble ions
94 accounting for 39% of total mass. Water-soluble ions were dominated by sulfate (39%)
95 and showed pronounced seasonal variations. The aerosol composition, size
96 distributions, and back trajectory analysis together indicated a mixed impact of both
97 mineral dust from arid areas of northwest China and anthropogenic emissions from
98 urban areas. However, previous extensive efforts to characterize the chemical
99 properties of aerosol particles in the Tibetan Plateau heavily rely on filter
100 measurements with the duration ranging from days to weeks, real-time measurement
101 of aerosol particle composition is still very limited. A recent study by Xu et al. (2014a)
102 deployed a high-resolution time-of-flight aerosol mass spectrometer (HR-ToF-AMS)
103 at an urban site in Lanzhou in northwest China. The submicron aerosol in the city was
104 dominated by organic aerosol (47%) with a large contribution from local traffic and

105 cooking emissions (40%). To our knowledge, there is no such real-time measurement
106 of aerosol particle composition with aerosol mass spectrometer at rural sites in the
107 Tibetan Plateau yet.

108 The study of new particle formation and growth events in the Tibetan Plateau is
109 also relatively new. Since 2004, a number of studies have been conducted to
110 investigate the new particle formation (NPF) and particle growth events in various
111 environments in China (Wu et al., 2007; Wiedensohler et al., 2009; Yue et al., 2010;
112 Zhang et al., 2011b; Wang et al., 2013a; Wang et al., 2013b). The NPF events were
113 frequently observed in urban cities, rural sites, coastal regions, and mountain sites.
114 Sulfuric acid was found to play a dominant role in both NPF and subsequent particle
115 growth, while organics makes an important contributor to particle growth (Yue et al.,
116 2010). The particle growth rates varied largely depending on sites and days, yet
117 generally fell within 1 – 20 nm hr⁻¹. Kivekas et al. (2009) conducted a long-term
118 measurement of particle number size distributions at Waliguan, a global baseline site
119 located approximately 140 km southwest of our sampling site. The annual average
120 particle number concentration was found to be higher than other rural sites in the
121 world. Despite this, the particle growth and its relationship to chemical species in the
122 Tibetan Plateau are rarely investigated and remain poorly understood.

123 In this study, an Aerodyne Aerosol Chemical Speciation Monitor (ACSM) was
124 first deployed at a national background monitoring site (Menyuan, Qinghai) in the
125 Tibetan Plateau for the real-time characterization of submicron aerosol composition
126 including organics, sulfate, nitrate, ammonium, and chloride from 5 September to 15
127 October, 2013. Collocated measurements including black carbon and particle number
128 size distributions were also conducted at the same site. Here we report the aerosol
129 composition and variations of submicron aerosols and investigate the sources of
130 organic aerosol with positive matrix factorization (PMF). In addition, the particle
131 growth events are also characterized and the roles of chemical species in particle
132 growth are elucidated.

133 **2 Experimental method**

134 **2.1 Sampling site**

135 The sampling site, i.e., the national atmospheric background monitoring station
136 (NBS) (37°36'30"N, 101°15'26"E, 3295 m a.s.l.) is located on the Daban Mountain in
137 Menyuan, Qinghai province (Fig. 1). The sampling site is characterized by a typical
138 Plateau continental climate with a pleasantly cool and short summer, and a long cold
139 winter. The annual average temperature is -1~-2° C, and the precipitation is 426 - 860
140 mm. In this study, ambient temperature averaged 4.9 °C (-8.7 - 17.9° C) and wind
141 speed varied largely with an average value of 3 m s⁻¹. In addition, several precipitation
142 events were also observed, particularly during the first half period of this study (Fig.
143 3). The diurnal profiles of meteorological conditions including temperature, relative
144 humidity, wind speed, and wind direction are shown in Fig. S1. The sampling site is
145 relatively pristine with most areas covered by typical Tibetan Plateau plants, e.g.,
146 *potentilla fruticosa* and *kobresia* etc. There are no strong local anthropogenic source
147 emissions in this area (~ 741 km² with a population of ~2000) except occasional
148 biomass burning events [due to burning of a large amount of straws in the middle of](#)
149 [September and cow dung at the end of the campaign \(Li et al., 2015\)](#). . The capital
150 city Xining of Qinghai province with a population of 2,290,000 is approximately 160
151 km south of the sampling site which is connected by a national road G227 with few
152 traffic vehicles.

153 **2.2 Instrumentation**

154 The field measurements were conducted from 5 September to 15 October 2013.
155 All the instruments were placed in an air-conditioned room with the temperature
156 maintaining at ~23 °C. The chemical compositions of non-refractory submicron
157 aerosol (NR-PM₁) species including organics (Org), sulfate (SO₄), nitrate (NO₃),
158 ammonium (NH₄) and chloride (Cl) were measured *in-situ* by an Aerodyne ACSM
159 (Ng et al., 2011b). A PM_{2.5} cyclone (Model: URG-2000-30ED) was supplied in front
160 of the sampling line to remove coarse particles larger than 2.5 μm. The ambient air
161 was drawn inside the room through a 1/2 inch (outer diameter) stainless steel tube
162 using an external pump (flow rate is ~3 L min⁻¹). The sampling height is
163 approximately 2 m, and the particle residence time in the sampling tube is ~ 5s. A
164 silica gel diffusion dryer was then used to dry aerosol particles before sampling into

165 the ACSM. After passing through a 100 μm critical orifice, aerosol particles between
166 30 nm – 1 μm are focused into a narrow particle beam via the aerodynamic lens in the
167 vacuum chamber, and then flash vaporized and ionized at a heated surface ($\sim 600^\circ\text{C}$).
168 The positive ions generated are finally analyzed by a commercial quadrupole mass
169 spectrometer. In this study, the mass spectrometer of ACSM was operated at a
170 scanning rate of 500 ms amu^{-1} from m/z 10 to 150. The time resolution is
171 approximately 15 min by alternating 6 cycles between the ambient air and
172 particle-free air. The detailed operation of ACSM has been given in Sun et al.(2012).

173 In addition to ACSM measurements, a Scanning Mobility Particle Sizer (TSI,
174 3936) equipped with a long Differential Mobility Analyzer (DMA) was
175 simultaneously operated to measure the particle number size distributions between
176 11.8 nm – 478.3 nm at a time resolution of 5 min. Other collocated measurements
177 included CO by a non-dispersive infrared analyser (M300EU), O₃ by a UV
178 photometric analyzer (Teledyne Instruments, Model 400EU), NO_x by a commercial
179 chemiluminescence analyzer (M200EU), and SO₂ by a pulsed UV fluorescence
180 analyzer (M100EU) and black carbon (BC) by an Aethalometer (AE31, Magee
181 Scientific Corp). The meteorological parameters, e.g., temperature, relative humidity,
182 pressure, visibility, precipitation, wind speed and wind direct were also recorded at
183 the same site. All the data are reported at ambient conditions in Beijing Standard Time.
184 Note that the concentrations would be a factor of approximately 1.5 of the current
185 values if the data are converted to mass loadings at standard temperature and pressure
186 (STP, 273K and 1013.25 hPa).

187 **2.3 Data analysis**

188 The ACSM data were analyzed within Igor Pro (WaveMetrics, Inc., Oregon USA)
189 using the standard ACSM data analysis software (v.1.5.3.0). The mass concentrations
190 and chemical composition of NR-PM₁ species were obtained using the default relative
191 ionization efficiency (RIE) that is 1.4, 1.2, 1.1 and 1.3 for organics, sulfate, nitrate and
192 chloride, respectively, except ammonium (6.5) that was derived from pure ammonium
193 nitrate during ionization efficiency (IE) calibration. A collection efficiency (CE) of 0.5
194 was used to account for the incomplete detection of aerosol species (Matthew et al.,

195 2008; Middlebrook et al., 2012) because aerosol particles were dry and only slightly
196 acidic, and also the mass fraction of ammonium nitrate is not high enough to affect
197 CE significantly.

198 The sources of organic aerosol were investigated by performing Positive Matrix
199 Factorization (PMF2.exe, v 4.2) on ACSM OA mass spectra (Paatero and Tapper,
200 1994; Ulbrich et al., 2009). PMF is a standard multivariate factor analysis model
201 broadly used in the field of air pollution source apportionment. The detailed PMF
202 analysis of organic aerosol from AMS measurements, including error matrix
203 preparation, data pretreatment, selections of the optimum number of factors and
204 rotational forcing parameter (FPEAK), and the evaluation of PMF solutions was given
205 in Ulbrich et al. (2009) and Zhang et al. (2011a). In this study, the organic mass
206 spectra from m/z 12 to m/z 125 were used for the PMF analysis. Because of the
207 absence of collocated measurements, the two factor solution with $f_{\text{peak}} = 0$ and
208 Q/Q_{exp} close to 1 was chosen (see Fig. S2 for the PMF diagnostic plots). The two
209 factors including a biomass burning OA (BBOA) and an oxygenated OA (OOA) were
210 identified. The two OA factors showed largely different factor profiles and time series
211 indicating their distinct sources.

212 **3 Results and discussion**

213 **3.1 Mass concentration and chemical composition of submicron aerosol**

214 Figure 2 shows a comparison of the total PM_{10} mass (NR- PM_{10} + BC) with that
215 determined from the SMPS measurements. Assuming spherical particles, the SMPS
216 number concentrations were converted to the mass concentrations using
217 chemically-resolved particle density that was estimated from the chemical
218 composition of PM_{10} (Salcedo et al., 2006). As shown in Fig. 2, the time series of PM_{10}
219 tracks well with that of SMPS measurements ($r^2 = 0.87$). The slope of 0.52 is likely
220 due to the limited size range of SMPS measurements (12 – 478 nm) by missing a
221 considerable fraction of large particles that ACSM can measure. The PM_{10} mass varied
222 dramatically throughout the study with hourly average concentration ranging from 1.0
223 to $78.4 \mu\text{g m}^{-3}$. The average mass concentration of PM_{10} ($\pm 1\sigma$) for the entire study is
224 $11.4 (\pm 8.5) \mu\text{g m}^{-3}$, which is ~3 – 4 times lower than those observed at rural sites in

225 China ($29.9 - 44.1 \mu\text{g m}^{-3}$) (Huang et al., 2011; Hu et al., 2013; Huang et al., 2013;
226 Zhang et al., 2014). It is also approximately twice lower than that ($24.5 \mu\text{g m}^{-3}$)
227 measured at an urban site in Lanzhou in the Tibetan Plateau in 2012 (Xu et al., 2014a).
228 While the average PM_{10} mass concentration in this study is close to those observed at
229 the remote sites in Asia, e.g., Okinawa ($14.5 \mu\text{g m}^{-3}$) (Zhang et al., 2007a) and Fukue
230 ($12.0 \mu\text{g m}^{-3}$) (Takami et al., 2005) in Japan in 2003, and Jeju ($8.6 \mu\text{g m}^{-3}$) in Korea in
231 2001 (Topping et al., 2004), it is much higher than those reported at rural/remote sites
232 in north America and Europe, e.g., Chebogue ($2.9 \mu\text{g m}^{-3}$), Storm Peak in 2004 (2.1
233 $\mu\text{g m}^{-3}$) and Hyytiala in 2005 ($2.0 \mu\text{g m}^{-3}$), and even comparable to the loadings at
234 urban sites, e.g., New York City in 2004 ($12 \mu\text{g m}^{-3}$), Pittsburgh ($15 \mu\text{g m}^{-3}$), and
235 Manchester in 2002 ($14.0 \mu\text{g m}^{-3}$) (Zhang et al., 2007a). These results suggest that the
236 Menyuan NBS is a typical rural site in Asia, yet with higher background
237 concentrations compared to those in other continents.

238 Figure 3 shows the time series of mass concentrations and mass fractions of
239 aerosol species in PM_{10} . The average PM_{10} composition is dominated by organics and
240 sulfate on average accounting for 43% and 28%, respectively. Black carbon and
241 chloride represent small fractions contributing 4.5% and 1.2%, respectively to PM_{10} .
242 As shown in Fig. 1, the aerosol composition at the Menyuan NBS is largely different
243 from that observed at the urban site in the Tibetan Plateau (Xu et al., 2014a). In
244 particular, sulfate shows ~60% higher contribution, yet BC is more than twice lower
245 than that observed at the urban site (Fig. 1). Xu et al. (2014a) found that 47% of BC
246 was from local traffic emissions which well explained the higher contribution of BC
247 at the urban site. Compared to this study, the average composition of PM_{10} measured
248 by the AMS at other rural sites in China showed similar dominance of sulfate (25 –
249 34%) except Changdao Island (19%), yet overall higher contributions of nitrate
250 because most these rural sites are close to urban areas with high NO_x emissions. The
251 sulfate contributions become more dominant (36 – 64%) at remote sites in East Asia
252 which are far away from urban areas. The increase of sulfate contribution is
253 associated with a large reduction of nitrate contribution (< 5%). Such a change in
254 aerosol bulk composition at rural/remote sites in East Asia is shown Fig. 1. Overall,

255 organics comprises the major fraction of PM₁, contributing approximately one third of
256 the total mass at most sites. While sulfate plays a dominant role in PM₁ at remote sites,
257 nitrate shows the highest contribution at the rural sites in eastern China. Such
258 compositional differences illustrate the different sources of sulfate and nitrate. While
259 sulfate is dominantly from regional sources and transport, nitrate is more likely
260 influenced by anthropogenic NO_x emissions over a smaller regional areas.

261 Aerosol species also varied dramatically throughout the study. For example, the
262 organics increased rapidly from 2.9 μg m⁻³ to 77.8 μg m⁻³ in one hour on 21
263 September. While sulfate remained small variations, nitrate, chloride, and BC showed
264 similar steep increases as organics indicating strong impacts of local biomass burning
265 (Zhang et al., 2015). Rapid decreases of aerosol species due to the precipitation of
266 scavenging or wind direction change were also frequently observed. For a better
267 understanding aerosol composition under variable meteorological conditions and
268 sources, five episodes with two of them from clean periods are shown in Fig. 3d. The
269 aerosol composition varied largely among different episodes. While the average PM₁
270 mass concentrations during the two clean episodes are similar (3.6 and 3.8 μg m⁻³),
271 the episode of Clean2 shows much higher contribution of organics (48% vs. 34%)
272 with slightly lower sulfate (33% vs. 36%) than Clean 1, consistent with their different
273 air mass trajectories (Fig. S3). The other three episodes show ~5 – 8 times higher
274 mass concentration of PM₁ (17.6 – 27.2 μg m⁻³) than the two clean episodes. The Ep1
275 is dominated by organics (70%), almost twice of those during the other two episodes
276 suggesting a largely different source. The relative contributions of sulfate and
277 organics during Ep2 and Ep3 are different although the nitrate contribution is similar.
278 These results suggest that the national background site is subject to the influences of
279 air masses from different sources, some of which are enriched with OA while others
280 are dominated with aerosols mainly composed of ammonium sulfates. We also
281 noticed that the two clean periods showed overall higher contribution of sulfate and
282 lower contribution of nitrate compared to the three pollution episodes. The possible
283 reasons were likely due to that the air masses during clean periods were either from a
284 longer transport when ammonium nitrate was deposited or evaporated due to dilution

285 processes, or from less anthropogenic influenced regions with low NO_x emissions.

286 The aerosol particle acidity was evaluated using the ratio of measured NH₄⁺
287 (NH₄⁺_{meas}) to the predicted NH₄⁺ (NH₄⁺_{pred} = 18×(2×SO₄⁻²/96+NO₃⁻/62+Cl⁻/35.5) that
288 needs to fully neutralize sulfate, nitrate, and chloride (Zhang et al., 2007b). The
289 NH₄⁺_{meas} correlates tightly with NH₄⁺_{pred} (r² = 0.95), yielding a regression slope of
290 0.80. The results suggest that aerosol particles at the Menyuan NBS are overall acidic.
291 Similar acidic particles were also observed at other rural sites in China, e.g., Jiaxing in
292 Yangtze River Delta (Huang et al., 2013), Kaiping in Pearl River Delta (Huang et al.,
293 2011), Yufa in Beijing (Takegawa et al., 2009), and Qilianshan Mountain in the
294 northeast of the Qinghai–Xizang Plateau (Xu et al., 2015). As a comparison, the
295 aerosol particles in the urban city Lanzhou in the Tibetan Plateau were overall
296 neutralized (Xu et al., 2014a). One of the explanations is that more SO₂ is oxidized to
297 sulfate during the transport while gaseous ammonia is not enough to neutralize the
298 newly formed sulfate. This is supported by the overall higher contribution of sulfate at
299 rural/remote sites than that at urban sites. Also note that the newly formed sulfate
300 particles during the frequent NPF events might also have played a role.

301 **3.2 Diurnal variations**

302 The diurnal cycles of aerosol species and PM₁ are shown in Fig. 4a. The PM₁
303 shows a pronounced diurnal cycle with the concentration ranging from 7.9 to 13.4 μg
304 m⁻³. The PM₁ shows a visible peak at noon time and then has a gradual decrease
305 reaching the minimum approximately at 16:00. After that, the PM₁ starts to build up
306 and reaches the highest level at midnight. Such a diurnal cycle is similar to those of
307 SO₂ and CO (Fig. 4d), which likely indicates that the major source of PM₁ at the
308 Menyuan NBS is from regional transport. All aerosol species present similarly
309 pronounced diurnal cycles to PM₁ with the lowest concentrations occurring
310 approximately at 16:00, indicating that the diurnal cycles of aerosol species were
311 mainly driven by the dynamics of planetary boundary layer. Organics dominated PM₁
312 composition throughout the day varying from 38% - 51%. The concentration of
313 organics at 16:00 is approximately twice lower than that at midnight. Sulfate shows
314 the largest noon peak among all aerosol species, consistent with those of SO₂ and CO.

315 The sulfate contributes more than 25% to PM₁ with the highest contribution as much
316 as 33% between 12:00 – 14:00. Nitrate and chloride shows relatively stable
317 concentrations before 11:00 and then gradually decreased to low ambient levels
318 during daytime. Such diurnal variations still exist after considering the dilution effects
319 of boundary layer height using the conserved tracer CO as a reference (Fig. 4c). This
320 indicates that gas-particle partitioning affected by temperature and humidity has
321 played an important role in driving the diurnal variations of nitrate and chloride.
322 Consistently, the nitrate contribution to PM₁ during late afternoon is ~7-8% which is
323 much lower than that (> 12%) in the early morning. The diurnal variation of BC is
324 different from that observed at the urban site in the Tibetan Plateau where the
325 pronounced morning peak due traffic influences was observed (Xu et al., 2014a). In
326 fact, BC has a good correlation with nitrate ($r^2 = 0.59$) indicating that BC is likely
327 dominantly from regional transport. This is also supported by the low ambient levels
328 of NO_x (2.5 – 5.1 μg m⁻³). The contribution of BC to PM₁ is relatively constant, which
329 is ~ 4 – 5% throughout the day.

330 **3.3 OA composition and sources**

331 PMF analysis of ACSM OA mass spectra identified two factors, i.e., a biomass
332 burning OA (BBOA) and an oxygenated OA (OOA). The mass spectra and time
333 series of the two OA factors are shown in Fig. 5.

334 **3.3.1 BBOA**

335 The mass spectrum of BBOA resembles to that of standard BBOA ($r^2 = 0.82$)
336 which is characterized by a prominent peak of m/z 60 (1.1% of total signal), a tracer
337 m/z for biomass burning aerosols (Aiken et al., 2009; Cubison et al., 2011; Hennigan
338 et al., 2011). The fraction of m/z 60 in BBOA (1.1%) is also much higher than ~0.3%
339 in the absence of biomass burning impacts (Cubison et al., 2011). BBOA correlates
340 tightly with m/z 60 ($r^2 = 0.82$) and also chloride ($r^2 = 0.52$). The ratio of BBOA to m/z
341 60 is 55.6, which is higher than that of fresh BBOA (34.5) measured during the
342 second Fire Lab at Missoula Experiment (FLAME II) (Lee et al., 2010). One of the
343 explanations is that BBOA in the ambient is more aged because the m/z 60 related
344 levoglucosan can be rapidly oxidized in the atmosphere (Hennigan et al., 2010).

345 Indeed, Zhang et al. (2015) reported a much higher ratio of aged BBOA to m/z 60
346 (74.8) than fresh BBOA (16.8) during two harvest seasons in Nanjing, China. The
347 time series of BBOA shows periodically large peaks, particularly on the days of 21
348 and 22 September, which were mainly from the burning of a large amount of straws in
349 the south-west region. Relatively high concentration of BBOA was also observed at
350 the end of the campaign due to the burning of cow dung for heating purpose because
351 of the low temperature. The average concentration of BBOA is $0.8 (\pm 1.5) \mu\text{g m}^{-3}$ for
352 the entire study on average accounting for 15% of total OA. Although the average
353 BBOA contribution is much lower than those measured in PRD, e.g., Jiaxing ($\sim 3.9 \mu\text{g m}^{-3}$,
354 30.1%) (Huang et al., 2013), Kaiping ($\sim 1.36 \mu\text{g m}^{-3}$, 24.5%) (Huang et al., 2011),
355 and Shenzhen ($\sim 5.2 \mu\text{g m}^{-3}$, 29.5%) (He et al., 2011), the contribution of BBOA
356 during some strong BB plumes can reach up to 40%, e.g., 21-22 September,
357 indicating a large impact of biomass burning on OA at the national background site.
358 BBOA showed a pronounced diurnal cycle which is similar to that of chloride (Fig.
359 5c). The BBOA concentration increased rapidly from 18:00 and reached a maximum
360 in 2 hours, likely indicating that the burning of straws and cow dung mainly occurred
361 during this period of time. As a result, the contribution of BBOA to total OA increased
362 from $\sim 10\%$ to more than 20%.

363 **3.3.2 Oxygenated organic aerosols (OOA)**

364 Similar to previously reported OOA (Zhang et al., 2005), the mass spectrum of
365 OOA in this study is characterized by a prominent m/z 44 peak (mainly CO_2^+). The
366 mass spectrum of OOA also resembles to that of low-volatility OOA ($r^2 = 0.88$) (Ng
367 et al., 2011a), yet with higher fraction of m/z 44 (f_{44}). Much higher fraction of m/z 44
368 in ACSM OOA spectrum than that from HR-ToF-AMS was reported recently by a
369 comprehensive evaluation of the ACSM (Fröhlich et al., 2015). The results also
370 showed that f_{44} has minor impacts on the mass concentrations of OOA factors,
371 although it varies largely by a factor of 0.6 – 1.3. The average mass concentration of
372 OOA is $4.1 \mu\text{g m}^{-3}$, on average accounting for 85% of total OA. The OOA
373 contribution is much higher than those reported at urban sites in summer ($\sim 60\%$)
374 (Huang et al., 2010; Sun et al., 2012; Xu et al., 2014a), and also higher than those

375 (~70%) observed at rural sites in China (Hu et al., 2013; Huang et al., 2013). These
376 results suggest that organic aerosol was highly aged and well processed at the
377 Menyuan NBS. In addition, aqueous-processing of OA at nighttime associated with
378 high RH might also played a role in forming the highly oxidized OA. The diurnal
379 cycle of OOA was similar to that of PM₁, which showed a small peak before noon
380 time followed by a subsequent decrease until 16:00. The OOA dominated OA
381 throughout the day varying from 80 – 90%, indicating that OA at the Menyuan NBS
382 was mainly composed of secondary organic aerosol.

383 Previous studies have shown the ubiquitously tight correlations between sulfate
384 and highly oxidized OA because of their similar secondary nature over regional scales
385 (Zhang et al., 2005; DeCarlo et al., 2010). While the OOA correlates well with
386 secondary sulfate for most of the time in this study, several periods with largely
387 different correlations were also observed (Fig. 6). As shown in Figs. 5b and 6, the
388 weak correlation events mainly occurred during periods with strong biomass burning
389 impacts were observed. However, it cannot be resolved by extending PMF solution to
390 more than 2 factors because of the limitation of PMF technique in source
391 apportionment analysis. Similar different correlations between sulfate and LV-OOA
392 were also observed during two research flights in Mexico City and the Central
393 Mexican Plateau (DeCarlo et al., 2010). Following the approach suggested by
394 DeCarlo et al. (2010), we performed a post-processing technique with external tracers
395 on the further apportionment of OOA. We first assume that OOA and sulfate have
396 similar sources during periods in the absence of biomass burning impacts, which is
397 supported by their tight correlations ($r^2 = 0.74$). An average OOA/SO₄ ratio of 1.04,
398 i.e., (OOA/SO₄)_{NBB}, was obtained by performing a linear regression analysis on OOA
399 versus SO₄. We then assume that SO₄ is completely from non-biomass burning (NBB)
400 sources during BB-impact periods. This assumption is rational because previous
401 studies have found that fresh biomass burning emits a very small or negligible
402 fraction of sulfate (Levin et al., 2010). The sulfate-related OOA can be calculated as
403 OOA × [OOA/SO₄]_{NBB}, and the excess OOA that is from different sources is then
404 determined as:

$$405 \quad \text{OOA}_{\text{post-processed}} = \text{OOA} - \text{SO}_4 \times [\text{OOA}/\text{SO}_4]_{\text{NBB}} \quad (1)$$

406 Because the post-processed OOA shows high concentrations during BB periods, we
 407 conclude that it's very likely an aged BBOA that was mixed with OOA. In fact, the
 408 mass spectrum of $\text{OOA}_{\text{post-processed}}$ is similar to that of OOA. The fraction of m/z 60 (f_{60})
 409 is 0.29%, which is very close to $\sim 0.3\%$ for non-biomass burning organic aerosol
 410 (Aiken et al., 2008). Smog chamber experiments have shown that fresh BBOA can be
 411 rapidly oxidized within 3 – 4.5 hours (Hennigan et al., 2011). While f_{44} increases
 412 significantly, f_{60} quickly decreases to a value close to $\sim 0.3\%$. Similarly, a recent study
 413 in Nanjing resolved an aged BBOA factor with its spectrum resembling to that of
 414 OOA yet with much lower f_{60} (Zhang et al., 2015). The average concentration of aged
 415 BBOA is $0.82 (\pm 2.65) \mu\text{g m}^{-3}$, accounting for 17% of OA for the entire study. The
 416 contribution of aged BBOA is close to that of fresh BBOA, which might indicate that
 417 half of BBOA has been aged. Still, the sum of fresh and aged BBOA highly correlates
 418 with m/z 60 ($r^2 = 0.81$, slope = 136.1). The fresh and aged BBOA together accounted
 419 for 33% of the total OA suggesting that BBOA was a large local source of OA during
 420 the observational period. With the post-processing technique, the sulfate-related OOA
 421 contributed 67% on average of total OA, which is close to those observed at other
 422 rural sites in e.g., Kaiping (Huang et al., 2011) and Changdao (Hu et al., 2013).

423 **3.4 Chemistry of particle growth**

424 Figure 7a shows the evolution of size distributions of particle number
 425 concentrations for the entire study. New particle formation and growth events (NPE)
 426 were observed almost every day (27 days in 34 days). Most NPE started at $\sim 11:00$
 427 (The time of sunrise is 2 hours behind of Beijing standard time) and persisted more
 428 than half day except some NPE were interrupted by either precipitation events or
 429 strong winds. The average particle number size distributions during NPE and non
 430 event days (non-NPE) are shown in Fig. 7b. Both NPE and non-NPE show broad size
 431 distributions with higher number concentrations occurring during NPE. Three modes
 432 with geometric mean diameter (GMD) peaking at 28 nm, 43 nm, and 104 nm,
 433 respectively were resolved using a log-normal distribution fitting (Seinfeld and Pandis,
 434 2006). The largest mode (104 nm) dominated the total number of particles accounting

435 for ~70%. In contrast, the average size distribution during non-NPE was characterized
436 by a bi-modal distribution with the GMD peaking at 59 nm and 146 nm, respectively.
437 The peak diameters were shifted to the larger sizes compared to those during NPE.
438 Such a size shift from clean days to polluted days was also observed previously in
439 Beijing (Yue et al., 2010). Also, the two modes showed almost equivalent
440 contributions to the total number of particles. The average particle number
441 concentration for the entire study is $2.4 \times 10^3 \text{ cm}^{-3}$, which is nearly an order of
442 magnitude lower than those reported at rural sites in eastern China (Wu et al., 2007),
443 but close to that ($2.03 \times 10^3 \text{ cm}^{-3}$) observed at Mount Waliguan which is a remote site
444 located nearby (Kivekas et al., 2009). The particle size was further segregated into
445 small Aitken mode (20 – 40 nm, N_{20-40}), large Aitken mode (40 – 100 nm, N_{40-100}),
446 and Accumulation mode (100 – 470 nm, N_{Accu}) particles. The time series and diurnal
447 cycles of particle numbers for three different sizes are shown in Fig. 7c, d. The N_{20-40}
448 presented sharp peaks almost in everyday corresponding to new particle formation
449 events. The diurnal cycle of N_{20-40} showed that the number concentration started to
450 increase at approximately 11:00 (150 cm^{-3}) and reached a maximum at 14:00 (770
451 cm^{-3}). In contrast, the N_{40-100} and N_{Accu} showed largely different diurnal cycles from
452 that of N_{20-40} , indicating their different sources. In fact, the diurnal cycles of N_{40-100}
453 and N_{Accu} are remarkably similar to those of aerosol species, suggesting that the large
454 particles are more likely from regional transport.

455 Figure 8 shows the diurnal evolution of particle number size distributions, aerosol
456 composition, and gaseous species during NPE and non-NPE days. The particle
457 number size distributions during NPE were characterized by distinct bimodal
458 distributions showing a persistent larger mode with the GMD peaking at ~100 nm,
459 and a smaller mode below 50 nm. The particle growth started at approximately 11:00
460 from ~20 nm, and continued to grow slowly until ~45 nm at mid-night. The maximum
461 size particles can grow in this study is generally smaller than those (~60 – 70 nm)
462 observed at urban and rural sites in Beijing (Wang et al., 2013a), which is likely due
463 to the much lower concentrations of aerosol species and precursors. All aerosol
464 species however showed decreases during the particle growth period between 12:00 –

465 17:00, and the gaseous CO and SO₂ showed similar variations as aerosol species. By
466 excluding the dilution effect of PBL using CO as a tracer, we found that organics was
467 the only species showing a gradual increase during the particle growth period (Fig. 8a)
468 while other species remained minor changes or even slightly decreased. The
469 contribution of organics to PM₁ also showed a corresponding increase from 40% to
470 47%. These results suggest that organics might have played a dominant role in
471 particle growth at the national background site. Our conclusion is consistent with the
472 recent findings that organics, particularly oxidized organic aerosol species, play a
473 more important role than ammonium sulfate in particle growth (Dusek et al., 2010;
474 Ehn et al., 2014; Setyan et al., 2014). Also note that the contribution of organics to
475 PM₁ during NPE (~40 – 50%) is overall higher than that during non-NPE (~30 –
476 40%), while the sulfate contribution is correspondingly lower (~20 – 30% vs. 30 –
477 40%), which further supports the important role of organics during NPE. The particle
478 growth was mixed with anthropogenic sources from 17:00 which are indicated by
479 synchronous enhancements of both aerosol species and gaseous precursors. One of
480 possible reasons is due to the air mass transport from downwind urban areas.

481 The diurnal evolution of particle size distributions and aerosol composition
482 during non-NPE is largely different from that during NPE. The particle number size
483 distributions and mass concentrations of aerosol species showed a dramatic variation
484 at noon time (12:00), indicating a very different chemical and/or physical process
485 between the first and the second half day. The aerosol particles showed an evident
486 growth from ~50 nm to 60 nm during the first 6 hours, which is likely a continuation
487 of previous NPE. Compared to the early stage of particle growth during NPE, the
488 particle growth during non-NPE is associated with synchronous increases of both
489 organics and sulfate. The results indicate that both organics and sulfate contribute to
490 the particle growth after mixed with anthropogenic sources from ~18:00 in the
491 previous day.

492 We further calculated the particle growth rates (GR) for NPE events without
493 interruptions due to meteorological changes using Eq. (2).

494
$$GR = \frac{\Delta D_m}{\Delta t} \quad (2)$$

495 Where D_m is the geometric mean diameter from the log-normal fitting, ΔD_m is the
496 difference of diameter during the growth period and Δt is the duration of growth time.
497 The calculated GR and the corresponding average chemical composition and fraction
498 of OOA during the growth period are shown in Fig. 9a. The GR ranges from 0.8 nm
499 h^{-1} to 3.2 nm h^{-1} with an average of 2.0 nm h^{-1} . The GR in this study is overall
500 consistent with those observed at remote and/or forest sites (Eisele and McMurry,
501 1997; Weber et al., 1997), yet generally smaller than those measured at urban and
502 polluted rural sites (Yue et al., 2010; Shen et al., 2011; Zhang et al., 2011b) where
503 abundant condensable vapor and high concentrations of particulate matter facilitate
504 the growth of particles (Wang et al., 2013a). By linking GR to aerosol composition,
505 we found that GR at the background site is positively related to the fraction of
506 oxidized OA, which likely indicate the important role of oxidized secondary organic
507 aerosol in particle growth (Ehn et al., 2014). Zhang et al. (2011b) also observed a
508 tight correlation between OOA and GR in urban Beijing supporting the important role
509 of OOA in particle growth. Further investigation is needed for a better understanding
510 of the role of organic aerosol, particularly oxidized OA, in the new particle formation
511 and particle growth at the regional background site.

512 **4 Conclusions**

513 The aerosol particle composition and particle number size distributions were
514 measured at a national background monitoring station in the Tibetan Plateau (3295 m,
515 a.s.l.) from 5 September to 15 October 2013. The average mass concentration of PM_{10}
516 is 11.4 (\pm 8.5) $\mu g m^{-3}$ for the entire study, which is lower than those observed at urban
517 and rural sites in eastern China. Organics constituted the major fraction of PM_{10} , on
518 average accounting for 43% followed by sulfate (28%) and ammonium (11%).
519 Several periods with the contribution of organics as much as 70% due to biomass
520 burning impacts were also observed. All aerosol species presented similar diurnal
521 cycles that were mainly driven by the dynamics of planetary boundary layer and
522 regional transport. PMF source apportionment analysis resolved a secondary OOA

523 and a primary BBOA. OOA dominated OA composition accounting for 85% on
524 average with the rest being BBOA. A post-processing technique based on the
525 correlation of OOA and sulfate separated an aged BBOA which on average accounted
526 for 17% of OA. New particle formation and particle growth events were frequently
527 observed during this study. The particle growth rates varied from 0.8 to 3.2 nm hr⁻¹
528 with an average growth rate of 2.0 nm hr⁻¹. Organics was found to be the only species
529 with gradually increased contribution to PM₁ during NPE. Also, higher contribution
530 of organics during NPE than non-NPE days was observed. These results potentially
531 illustrate the important role of organics in particle growth. Further analysis showed a
532 positive correlation of particle growth rate with the fraction of OOA suggesting that
533 oxidized OA plays a critical role contributing to the particle growth.

534

535 **Acknowledgements**

536 This work was supported by the National Natural Science Foundation of China
537 (41375133), the National Key Project of Basic Research (2013CB955801), and the
538 Strategic Priority Research Program (B) of the Chinese Academy of Sciences (Grant
539 No. XDB05020501). We thank the National Station for Background Atmospheric
540 Monitoring for providing the meteorological data and gaseous data.

541

542 **References**

543 Aiken, A. C., DeCarlo, P. F., Kroll, J. H., Worsnop, D. R., Huffman, J. A., Docherty, K.
544 S., Ulbrich, I. M., Mohr, C., Kimmel, J. R., Sueper, D., Sun, Y., Zhang, Q.,
545 Trimborn, A., Northway, M., Ziemann, P. J., Canagaratna, M. R., Onasch, T. B.,
546 Alfarra, M. R., Prevot, A. S. H., Dommen, J., Duplissy, J., Metzger, A.,
547 Baltensperger, U., and Jimenez, J. L.: O/C and OM/OC ratios of primary,
548 secondary, and ambient organic aerosols with High-Resolution Time-of-Flight
549 Aerosol Mass Spectrometry, *Environ. Sci. Technol.*, 42, 4478-4485, 2008.
550 Aiken, A. C., Salcedo, D., Cubison, M. J., Huffman, J. A., DeCarlo, P. F., Ulbrich, I.
551 M., Docherty, K. S., Sueper, D., Kimmel, J. R., Worsnop, D. R., Trimborn, A.,
552 Northway, M., Stone, E. A., Schauer, J. J., Volkamer, R. M., Fortner, E., de Foy, B.,
553 Wang, J., Laskin, A., Shutthanandan, V., Zheng, J., Zhang, R., Gaffney, J., Marley,
554 N. A., Paredes-Miranda, G., Arnott, W. P., Molina, L. T., Sosa, G., and Jimenez, J.
555 L.: Mexico City aerosol analysis during MILAGRO using high resolution aerosol
556 mass spectrometry at the urban supersite (T0) - Part 1: Fine particle composition

557 and organic source apportionment, *Atmos. Chem. Phys.*, 9, 6633-6653, 2009.

558 Cao, J., Lee, S., Chow, J. C., Watson, J. G., Ho, K., Zhang, R., Jin, Z., Shen, Z., Chen,
559 G., and Kang, Y.: Spatial and seasonal distributions of carbonaceous aerosols over
560 China, *J. Geophys. Res.*, 112, 2007.

561 Cong, Z., Kang, S., Kawamura, K., Liu, B., Wan, X., Wang, Z., Gao, S., and Fu, P.:
562 Carbonaceous aerosols on the south edge of the Tibetan Plateau: concentrations,
563 seasonality and sources, *Atmos. Chem. Phys.*, 15, 1573-1584,
564 10.5194/acp-15-1573-2015, 2015.

565 Cubison, M. J., Ortega, A. M., Hayes, P. L., Farmer, D. K., Day, D., Lechner, M. J.,
566 Brune, W. H., Apel, E., Diskin, G. S., Fisher, J. A., Fuelberg, H. E., Hecobian, A.,
567 Knapp, D. J., Mikoviny, T., Riemer, D., Sachse, G. W., Sessions, W., Weber, R. J.,
568 Weinheimer, A. J., Wisthaler, A., and Jimenez, J. L.: Effects of aging on organic
569 aerosol from open biomass burning smoke in aircraft and laboratory studies,
570 *Atmos. Chem. Phys.*, 11, 12049-12064, 10.5194/acp-11-12049-2011, 2011.

571 DeCarlo, P. F., Ulbrich, I. M., Crounse, J., de Foy, B., Dunlea, E. J., Aiken, A. C.,
572 Knapp, D., Weinheimer, A. J., Campos, T., Wennberg, P. O., and Jimenez, J. L.:
573 Investigation of the sources and processing of organic aerosol over the Central
574 Mexican Plateau from aircraft measurements during MILAGRO, *Atmos. Chem.*
575 *Phys.*, 10, 5257-5280, 10.5194/acp-10-5257-2010, 2010.

576 Dusek, U., Frank, G. P., Curtius, J., Drewnick, F., Schneider, J., Kürten, A., Rose, D.,
577 Andreae, M. O., Borrmann, S., and Pöschl, U.: Enhanced organic mass fraction
578 and decreased hygroscopicity of cloud condensation nuclei (CCN) during new
579 particle formation events, *Geophys. Res. Lett.*, 37, L03804,
580 10.1029/2009gl040930, 2010.

581 Ehn, M., Thornton, J. A., Kleist, E., Sipila, M., Junninen, H., Pullinen, I., Springer, M.,
582 Rubach, F., Tillmann, R., Lee, B., Lopez-Hilfiker, F., Andres, S., Acir, I.-H.,
583 Rissanen, M., Jokinen, T., Schobesberger, S., Kangasluoma, J., Kontkanen, J.,
584 Nieminen, T., Kurten, T., Nielsen, L. B., Jorgensen, S., Kjaergaard, H. G.,
585 Canagaratna, M., Maso, M. D., Berndt, T., Petaja, T., Wahner, A., Kerminen,
586 V.-M., Kulmala, M., Worsnop, D. R., Wildt, J., and Mentel, T. F.: A large source of
587 low-volatility secondary organic aerosol, *Nature*, 506, 476-479,
588 10.1038/nature13032, 2014.

589 Eisele, F. L., and McMurry, P. H.: Recent progress in understanding particle
590 nucleation and growth, *Philosophical Transactions of the Royal Society B:*
591 *Biological Sciences*, 352, 191-201, 10.1098/rstb.1997.0014, 1997.

592 Fröhlich, R., Crenn, V., Setyan, A., Belis, C. A., Canonaco, F., Favez, O., Riffault, V.,
593 Slowik, J. G., Aas, W., Aijälä, M., Alastuey, A., Artiñano, B., Bonnaire, N.,
594 Bozzetti, C., Bressi, M., Carbone, C., Coz, E., Croteau, P. L., Cubison, M. J.,
595 Esser-Gietl, J. K., Green, D. C., Gros, V., Heikkinen, L., Herrmann, H., Jayne, J.
596 T., Lunder, C. R., Minguillón, M. C., Močnik, G., O'Dowd, C. D., Ovadnevaite, J.,
597 Petralia, E., Poulain, L., Priestman, M., Ripoll, A., Sarda-Estève, R., Wiedensohler,
598 A., Baltensperger, U., Sciare, J., and Prévôt, A. S. H.: ACTRIS ACSM
599 intercomparison – Part 2: Intercomparison of ME-2 organic source apportionment
600 results from 15 individual, co-located aerosol mass spectrometers, *Atmos. Meas.*

601 Tech. Discuss., 8, 1559-1613, 10.5194/amtd-8-1559-2015, 2015.

602 Gong, Z., Lan, Z., Xue, L., Zeng, L., He, L., and Huang, X.: Characterization of
603 submicron aerosols in the urban outflow of the central Pearl River Delta region of
604 China, *Front. Environ. Sci. Eng.*, 10.1007/s11783-012-0441-8, 2012.

605 He, L.-Y., Huang, X.-F., Xue, L., Hu, M., Lin, Y., Zheng, J., Zhang, R., and Zhang,
606 Y.-H.: Submicron aerosol analysis and organic source apportionment in an urban
607 atmosphere in Pearl River Delta of China using high-resolution aerosol mass
608 spectrometry, *J. Geophys. Res.*, 116, 10.1029/2010jd014566, 2011.

609 Hennigan, C. J., Sullivan, A. P., Collett, J. L., and Robinson, A. L.: Levoglucosan
610 stability in biomass burning particles exposed to hydroxyl radicals, *Geophys. Res.
611 Lett.*, 37, L09806, doi:10.1029/2010GL043088, 2010.

612 Hennigan, C. J., Miracolo, M. A., Engelhart, G. J., May, A. A., Presto, A. A., Lee, T.,
613 Sullivan, A. P., McMeeking, G. R., Coe, H., Wold, C. E., Hao, W. M., Gilman, J.
614 B., Kuster, W. C., de Gouw, J., Schichtel, B. A., Collett, J. L., Kreidenweis, S. M.,
615 and Robinson, A. L.: Chemical and physical transformations of organic aerosol
616 from the photo-oxidation of open biomass burning emissions in an environmental
617 chamber, *Atmos. Chem. Phys.*, 11, 7669-7686, 10.5194/acp-11-7669-2011, 2011.

618 Hu, W. W., Hu, M., Yuan, B., Jimenez, J. L., Tang, Q., Peng, J. F., Hu, W., Shao, M.,
619 Wang, M., Zeng, L. M., Wu, Y. S., Gong, Z. H., Huang, X. F., and He, L. Y.:
620 Insights on organic aerosol aging and the influence of coal combustion at a
621 regional receptor site of central eastern China, *Atmos. Chem. Phys.*, 13,
622 10095-10112, 10.5194/acp-13-10095-2013, 2013.

623 Huang, X.-F., Xue, L., Tian, X.-D., Shao, W.-W., Sun, T.-L., Gong, Z.-H., Ju, W.-W.,
624 Jiang, B., Hu, M., and He, L.-Y.: Highly time-resolved carbonaceous aerosol
625 characterization in Yangtze River Delta of China: composition, mixing state and
626 secondary formation, *Atmos. Environ.*, 64, 200 - 207,
627 10.1016/j.atmosenv.2012.09.059, 2013.

628 Huang, X. F., He, L. Y., Hu, M., Canagaratna, M. R., Sun, Y., Zhang, Q., Zhu, T., Xue,
629 L., Zeng, L. W., Liu, X. G., Zhang, Y. H., Jayne, J. T., Ng, N. L., and Worsnop, D.
630 R.: Highly time-resolved chemical characterization of atmospheric submicron
631 particles during 2008 Beijing Olympic Games using an Aerodyne
632 High-Resolution Aerosol Mass Spectrometer, *Atmos. Chem. Phys.*, 10, 8933-8945,
633 10.5194/acp-10-8933-2010, 2010.

634 Huang, X. F., He, L. Y., Hu, M., Canagaratna, M. R., Kroll, J. H., Ng, N. L., Zhang, Y.
635 H., Lin, Y., Xue, L., Sun, T. L., Liu, X. G., Shao, M., Jayne, J. T., and Worsnop, D.
636 R.: Characterization of submicron aerosols at a rural site in Pearl River Delta of
637 China using an Aerodyne High-Resolution Aerosol Mass Spectrometer, *Atmos.
638 Chem. Phys.*, 11, 1865-1877, 10.5194/acp-11-1865-2011, 2011.

639 Huang, X. F., He, L. Y., Xue, L., Sun, T. L., Zeng, L. W., Gong, Z. H., Hu, M., and
640 Zhu, T.: Highly time-resolved chemical characterization of atmospheric fine
641 particles during 2010 Shanghai World Expo, *Atmos. Chem. Phys.*, 12, 4897-4907,
642 10.5194/acp-12-4897-2012, 2012.

643 Jacobson, M. Z.: Strong radiative heating due to the mixing state of black carbon in
644 atmospheric aerosols, *Nature*, 409, 695-697,

645 http://www.nature.com/nature/journal/v409/n6821/supinfo/409695a0_S1.html,
646 2001.

647 Jiang, Q., Sun, Y. L., Wang, Z., and Yin, Y.: Aerosol composition and sources during
648 the Chinese Spring Festival: fireworks, secondary aerosol, and holiday effects,
649 *Atmos. Chem. Phys.*, 15, 6023-6034, 10.5194/acp-15-6023-2015, 2015.

650 Kivekas, N., Sun, J., Zhan, M., Kerminen, V. M., Hyvärinen, A., Komppula, M.,
651 Viisanen, Y., Hong, N., Zhang, Y., Kulmala, M., Zhang, X. C., Deli, G., and
652 Lihavainen, H.: Long term particle size distribution measurements at Mount
653 Waliguan, a high-altitude site in inland China, *Atmos. Chem. Phys.*, 9, 5461-5474,
654 2009.

655 Lee, T., Sullivan, A. P., Mack, L., Jimenez, J. L., Kreidenweis, S. M., Onasch, T. B.,
656 Worsnop, D. R., Malm, W., Wold, C. E., Hao, W. M., and Collett, J. L.: Chemical
657 Smoke Marker Emissions During Flaming and Smoldering Phases of Laboratory
658 Open Burning of Wildland Fuels, *Aerosol Sci. Technol.*, 44, i-v,
659 10.1080/02786826.2010.499884, 2010.

660 Levin, E. J. T., McMeeking, G. R., Carrico, C. M., Mack, L. E., Kreidenweis, S. M.,
661 Wold, C. E., Moosmüller, H., Arnott, W. P., Hao, W. M., Collett, J. L., Jr., and
662 Malm, W. C.: Biomass burning smoke aerosol properties measured during Fire
663 Laboratory at Missoula Experiments (FLAME), *J. Geophys. Res.*, 115, D18210,
664 10.1029/2009jd013601, 2010.

665 Li, J. J., Wang, G. H., Wang, X. M., Cao, J. J., Sun, T., Cheng, C. L., Meng, J. J., Hu,
666 T. F., and Liu, S. X.: Abundance, composition and source of atmospheric PM 2.5
667 at a remote site in the Tibetan Plateau, China, *Tellus B*, 65, 2013.

668 Li, W. J., Chen, S. R., Xu, Y. S., Guo, X. C., Sun, Y. L., Yang, X. Y., Wang, Z. F.,
669 Zhao, X. D., Chen, J. M., and Wang, W. X.: Mixing state, composition, and
670 sources of fine aerosol particles in the Qinghai-Tibetan Plateau and the influence
671 of agricultural biomass burning, *Atmos. Chem. Phys. Discuss.*, 15, 24369-24401,
672 10.5194/acpd-15-24369-2015, 2015.

673 Matthew, B. M., Middlebrook, A. M., and Onasch, T. B.: Collection efficiencies in an
674 Aerodyne Aerosol Mass Spectrometer as a function of particle phase for
675 laboratory generated aerosols, *Aerosol Sci. Technol.*, 42, 884-898,
676 10.1080/02786820802356797, 2008.

677 Middlebrook, A. M., Bahreini, R., Jimenez, J. L., and Canagaratna, M. R.: Evaluation
678 of Composition-Dependent Collection Efficiencies for the Aerodyne Aerosol Mass
679 Spectrometer using Field Data, *Aerosol Sci. Technol.*, 46, 258-271,
680 10.1080/02786826.2011.620041, 2012.

681 Ng, N. L., Canagaratna, M. R., Jimenez, J. L., Zhang, Q., Ulbrich, I. M., and Worsnop,
682 D. R.: Real-time methods for estimating organic component mass concentrations
683 from Aerosol Mass Spectrometer data, *Environ. Sci. Technol.*, 45, 910-916,
684 10.1021/es102951k, 2011a.

685 Ng, N. L., Herndon, S. C., Trimborn, A., Canagaratna, M. R., Croteau, P. L., Onasch,
686 T. B., Sueper, D., Worsnop, D. R., Zhang, Q., Sun, Y. L., and Jayne, J. T.: An
687 Aerosol Chemical Speciation Monitor (ACSM) for Routine Monitoring of the
688 Composition and Mass Concentrations of Ambient Aerosol, *Aerosol Sci. Technol.*,

689 45, 780-794, 10.1080/02786826.2011.560211, 2011b.

690 Paatero, P., and Tapper, U.: POSITIVE MATRIX FACTORIZATION - A
691 NONNEGATIVE FACTOR MODEL WITH OPTIMAL UTILIZATION OF
692 ERROR-ESTIMATES OF DATA VALUES, *Environmetrics*, 5, 111-126,
693 10.1002/env.3170050203, 1994.

694 Salcedo, D., Onasch, T. B., Dzepina, K., Canagaratna, M., Zhang, Q., Huffman, J.,
695 DeCarlo, P., Jayne, J., Mortimer, P., and Worsnop, D. R.: Characterization of
696 ambient aerosols in Mexico City during the MCMA-2003 campaign with Aerosol
697 Mass Spectrometry: results from the CENICA Supersite, *Atmos. Chem. Phys.*, 6,
698 925-946, 2006.

699 Seinfeld, J. H., and Pandis, S. N.: *Atmos. Chem. Phys.: from Air Pollution to Climate*
700 *Change*, Wiley, John & Sons, Incorporated, New York, 1203 pp., 2006.

701 Setyan, A., Song, C., Merkel, M., Knighton, W. B., Onasch, T. B., Canagaratna, M. R.,
702 Worsnop, D. R., Wiedensohler, A., Shilling, J. E., and Zhang, Q.: Chemistry of
703 new particle growth in mixed urban and biogenic emissions – insights from
704 CARES, *Atmos. Chem. Phys.*, 14, 6477-6494, 10.5194/acp-14-6477-2014, 2014.

705 Shen, X. J., Sun, J. Y., Zhang, Y. M., Wehner, B., Nowak, A., Tuch, T., Zhang, X. C.,
706 Wang, T. T., Zhou, H. G., Zhang, X. L., Dong, F., Birmili, W., and Wiedensohler,
707 A.: First long-term study of particle number size distributions and new particle
708 formation events of regional aerosol in the North China Plain, *Atmos. Chem.*
709 *Phys.*, 11, 1565-1580, 10.5194/acp-11-1565-2011, 2011.

710 Sun, J., Zhang, Q., Canagaratna, M. R., Zhang, Y., Ng, N. L., Sun, Y., Jayne, J. T.,
711 Zhang, X., Zhang, X., and Worsnop, D. R.: Highly time- and size-resolved
712 characterization of submicron aerosol particles in Beijing using an Aerodyne
713 Aerosol Mass Spectrometer, *Atmos. Environ.*, 44, 131-140, 2010.

714 Sun, Y. L., Wang, Z., Dong, H., Yang, T., Li, J., Pan, X., Chen, P., and Jayne, J. T.:
715 Characterization of summer organic and inorganic aerosols in Beijing, China with
716 an Aerosol Chemical Speciation Monitor, *Atmos. Environ.*, 51, 250-259,
717 10.1016/j.atmosenv.2012.01.013, 2012.

718 Sun, Y. L., Wang, Z. F., Fu, P. Q., Yang, T., Jiang, Q., Dong, H. B., Li, J., and Jia, J. J.:
719 Aerosol composition, sources and processes during wintertime in Beijing, China,
720 *Atmos. Chem. Phys.*, 13, 4577-4592, 10.5194/acp-13-4577-2013, 2013.

721 Sun, Y. L., Jiang, Q., Wang, Z., Fu, P., Li, J., Yang, T., and Yin, Y.: Investigation of
722 the sources and evolution processes of severe haze pollution in Beijing in January
723 2013, *J. Geophys. Res.*, 119, 4380-4398, 10.1002/2014JD021641, 2014.

724 Takami, A., Miyoshi, T., Shimono, A., and Hatakeyama, S.: Chemical composition of
725 fine aerosol measured by AMS at Fukue Island, Japan during APEX period,
726 *Atmos. Environ.*, 39, 4913-4924, 2005.

727 Takegawa, N., Miyakawa, T., Kuwata, M., Kondo, Y., Zhao, Y., Han, S., Kita, K.,
728 Miyazaki, Y., Deng, Z., Xiao, R., Hu, M., van Pinxteren, D., Herrmann, H.,
729 Hofzumahaus, A., Holland, F., Wahner, A., Blake, D. R., Sugimoto, N., and Zhu,
730 T.: Variability of submicron aerosol observed at a rural site in Beijing in the
731 summer of 2006, *J. Geophys. Res.*, 114, D00G05, 10.1029/2008jd010857, 2009.

732 Tie, X., and Cao, J.: Aerosol pollution in China: Present and future impact on

733 environment, *Particuology*, 7, 426-431,
734 <http://dx.doi.org/10.1016/j.partic.2009.09.003>, 2009.

735 Topping, D., Coe, H., McFiggans, G., Burgess, R., Allan, J., Alfarra, M. R., Bower, K.,
736 Choularton, T. W., Decesari, S., and Facchini, M. C.: Aerosol chemical
737 characteristics from sampling conducted on the Island of Jeju, Korea during ACE
738 Asia, *Atmos. Environ.*, 38, 2111-2123, 10.1016/j.atmosenv.2004.01.022, 2004.

739 Ulbrich, I. M., Canagaratna, M. R., Zhang, Q., Worsnop, D. R., and Jimenez, J. L.:
740 Interpretation of organic components from Positive Matrix Factorization of
741 aerosol mass spectrometric data, *Atmos. Chem. Phys.*, 9, 2891-2918, 2009.

742 Wan, X., Kang, S. C., Wang, Y. S., Xin, J. Y., Liu, B., Guo, Y. H., Wen, T. X., Zhang,
743 G. S., and Cong, Z. Y.: Size distribution of carbonaceous aerosols at a
744 high-altitude site on the central Tibetan Plateau (Nam Co Station, 4730 m a.s.l.),
745 *Atmospheric Research*, 153, 155-164, 10.1016/j.atmosres.2014.08.008, 2015.

746 Wang, Z. B., Hu, M., Sun, J. Y., Wu, Z. J., Yue, D. L., Shen, X. J., Zhang, Y. M., Pei,
747 X. Y., Cheng, Y. F., and Wiedensohler, A.: Characteristics of regional new particle
748 formation in urban and regional background environments in the North China
749 Plain, *Atmos. Chem. Phys.*, 13, 12495-12506, 10.5194/acp-13-12495-2013,
750 2013a.

751 Wang, Z. B., Hu, M., Wu, Z. J., Yue, D. L., He, L. Y., Huang, X. F., Liu, X. G., and
752 Wiedensohler, A.: Long-term measurements of particle number size distributions
753 and the relationships with air mass history and source apportionment in the
754 summer of Beijing, *Atmos. Chem. Phys.*, 13, 10159-10170,
755 10.5194/acp-13-10159-2013, 2013b.

756 Weber, R. J., Marti, J. J., McMurry, P. H., Eisele, F. L., Tanner, D. J., and Jefferson, A.:
757 Measurements of new particle formation and ultrafine particle growth rates at a
758 clean continental site, *J. Geophys. Res.*, 102, 4375, 10.1029/96jd03656, 1997.

759 Wiedensohler, A., Cheng, Y. F., Nowak, A., Wehner, B., Achtert, P., Berghof, M.,
760 Birmili, W., Wu, Z. J., Hu, M., Zhu, T., Takegawa, N., Kita, K., Kondo, Y., Lou, S.
761 R., Hofzumahaus, A., Holland, F., Wahner, A., Gunthe, S. S., Rose, D., Su, H., and
762 Poschl, U.: Rapid aerosol particle growth and increase of cloud condensation
763 nucleus activity by secondary aerosol formation and condensation: A case study
764 for regional air pollution in northeastern China, *J. Geophys. Res.-Atmos.*, 114,
765 D00g08, 10.1029/2008jd010884, 2009.

766 Wu, Z., Hu, M., Liu, S., Wehner, B., Bauer, S., Maßling, A., Wiedensohler, A., Petäjä,
767 T., Dal Maso, M., and Kulmala, M.: New particle formation in Beijing, China:
768 Statistical analysis of a 1-year data set, *J. Geophys. Res.*, 112,
769 10.1029/2006jd007406, 2007.

770 Xu, J., Zhang, Q., Chen, M., Ge, X., Ren, J., and Qin, D.: Chemical composition,
771 sources, and processes of urban aerosols during summertime in northwest China:
772 insights from high-resolution aerosol mass spectrometry, *Atmos. Chem. Phys.*, 14,
773 12593-12611, 10.5194/acp-14-12593-2014, 2014a.

774 Xu, J. Z., Wang, Z. B., Yu, G. M., Qin, X., Ren, J. W., and Qin, D.: Characteristics of
775 water soluble ionic species in fine particles from a high altitude site on the
776 northern boundary of Tibetan Plateau: Mixture of mineral dust and anthropogenic

777 aerosol, *Atmos. Res.*, 143, 43-56, 10.1016/j.atmosres.2014.01.018, 2014b.

778 Xu, J. Z., Zhang, Q., Wang, Z. B., Yu, G. M., Ge, X. L., and Qin, X.: Chemical
779 composition and size distribution of summertime PM_{2.5} at a high altitude remote
780 location in the northeast of the Qinghai–Xizang (Tibet) Plateau: insights into
781 aerosol sources and processing in free troposphere, *Atmos. Chem. Phys.*, 15,
782 5069-5081, 10.5194/acp-15-5069-2015, 2015.

783 Yue, D. L., Hu, M., Zhang, R. Y., Wang, Z. B., Zheng, J., Wu, Z. J., Wiedensohler, A.,
784 He, L. Y., Huang, X. F., and Zhu, T.: The roles of sulfuric acid in new particle
785 formation and growth in the mega-city of Beijing, *Atmos. Chem. Phys.*, 10,
786 4953-4960, 10.5194/acp-10-4953-2010, 2010.

787 Zhang, Q., Worsnop, D. R., Canagaratna, M. R., and Jimenez, J. L.: Hydrocarbon-like
788 and oxygenated organic aerosols in Pittsburgh: Insights into sources and processes
789 of organic aerosols, *Atmos. Chem. Phys.*, 5, 3289-3311, 2005.

790 Zhang, Q., Jimenez, J. L., Canagaratna, M. R., Allan, J. D., Coe, H., Ulbrich, I.,
791 Alfarra, M. R., Takami, A., Middlebrook, A. M., Sun, Y. L., Dzepina, K., Dunlea,
792 E., Docherty, K., DeCarlo, P. F., Salcedo, D., Onasch, T., Jayne, J. T., Miyoshi, T.,
793 Shimono, A., Hatakeyama, S., Takegawa, N., Kondo, Y., Schneider, J., Drewnick,
794 F., Borrmann, S., Weimer, S., Demerjian, K., Williams, P., Bower, K., Bahreini, R.,
795 Cottrell, L., Griffin, R. J., Rautiainen, J., Sun, J. Y., Zhang, Y. M., and Worsnop, D.
796 R.: Ubiquity and dominance of oxygenated species in organic aerosols in
797 anthropogenically-influenced Northern Hemisphere midlatitudes, *Geophys. Res.*
798 *Lett.*, 34, L13801, 10.1029/2007gl029979, 2007a.

799 Zhang, Q., Jimenez, J. L., Worsnop, D. R., and Canagaratna, M.: A case study of
800 urban particle acidity and its effect on secondary organic aerosol, *Environ. Sci.*
801 *Technol.*, 41, 3213-3219, 2007b.

802 Zhang, Q., Jimenez, J. L., Canagaratna, M. R., Ulbrich, I. M., Ng, N. L., Worsnop, D.
803 R., and Sun, Y.: Understanding atmospheric organic aerosols via factor analysis of
804 aerosol mass spectrometry: a review, *Anal. Bioanal. Chem.*, 401, 3045-3067,
805 10.1007/s00216-011-5355-y, 2011a.

806 Zhang, Y. J., Tang, L. L., Wang, Z., Yu, H. X., Sun, Y. L., Liu, D., Qin, W., Canonaco,
807 F., Prévôt, A. S. H., Zhang, H. L., and Zhou, H. C.: Insights into characteristics,
808 sources, and evolution of submicron aerosols during harvest seasons in the
809 Yangtze River delta region, China, *Atmos. Chem. Phys.*, 15, 1331-1349,
810 10.5194/acp-15-1331-2015, 2015.

811 Zhang, Y. M., Zhang, X. Y., Sun, J. Y., Lin, W. L., Gong, S. L., Shen, X. J., and Yang,
812 S.: Characterization of new particle and secondary aerosol formation during
813 summertime in Beijing, China, *Tellus B*, 63, 382-394,
814 10.1111/j.1600-0889.2011.00533.x, 2011b.

815 Zhang, Y. M., Zhang, X. Y., Sun, J. Y., Hu, G. Y., Shen, X. J., Wang, Y. Q., Wang, T. T.,
816 Wang, D. Z., and Zhao, Y.: Chemical composition and mass size distribution of
817 PM₁ at an elevated site in central east China, *Atmos. Chem. Phys.*, 14,
818 12237-12249, 10.5194/acp-14-12237-2014, 2014.

819 Zhao, Z. Z., Cao, J. J., Shen, Z. X., Xu, B. Q., Zhu, C. S., Chen, L. W. A., Su, X. L.,
820 Liu, S. X., Han, Y. M., Wang, G. H., and Ho, K. F.: Aerosol particles at a

821 high-altitude site on the Southeast Tibetan Plateau, China: Implications for
822 pollution transport from South Asia, *J. Geophys. Res.-Atmos.*, 118, 11360-11375,
823 10.1002/jgrd.50599, 2013.

824 **Tables**

825 Table 1. A summary of average mass concentrations ($\mu\text{g m}^{-3}$) of PM_{10} species during
826 five episodes and the entire study. The 30 min detection limit (DLs) of the ACSM is
827 also shown (Sun et al., 2012).

828

	Org	SO ₄	NO ₃	NH ₄	Cl	BC	PM ₁₀
Entire Study	4.9	3.2	1.2	1.4	0.14	0.51	11.4
Clean1	1.2	1.3	0.25	0.58	0.02	0.22	3.6
Clean2	1.8	1.3	0.24	0.45	0.03	-	3.8
Ep1	19.1	2.1	2.7	1.4	0.53	1.4	27.2
Ep2	6.3	5.9	2.0	2.6	0.18	0.57	17.6
Ep3	10.8	6.0	2.9	2.6	0.39	1.0	23.7
DLs	0.54	0.07	0.06	0.25	0.03		

829

830

831 **Figure Captions:**

832 Figure 1. Map of the sampling site (Menyuan, Qinghai). Also shown is the chemical
833 composition of submicron aerosols (NR-PM₁ + BC if it was available) measured at
834 selected rural/remote sites in East Asia except Lanzhou, an urban site in northwest
835 China. The two dotted blue lines are used to guide eyes for the three rural/remote
836 regions from the west to the east. The detailed information of the sampling sites is
837 presented in Table S1.

838 Figure 2. Comparison of the mass concentrations of PM₁ (NR-PM₁ +BC) measured
839 by the ACSM and Aethalometer with that by the SMPS ($D_m = 12 - 478$ nm): (a) time
840 series and (b) scatter plot.

841 Figure 3. Time series of (a-c) meteorological variables including T (temperature), RH
842 (relative humidity), Precip. (precipitation), WS (wind speed), WD (wind direction),
843 and Vis (visibility), (d) mass concentrations and (e) mass fractions of PM₁ species .
844 The pie charts show the average chemical composition of PM₁ for five episodes.

845 Figure 4. Average diurnal cycles of (a) mass concentration; (b) mass fraction of PM₁
846 species; (c) ratios of aerosol species to CO, and (d) gaseous species. The local sunrise
847 and sunset was around 7:00 and 19:00, respectively.

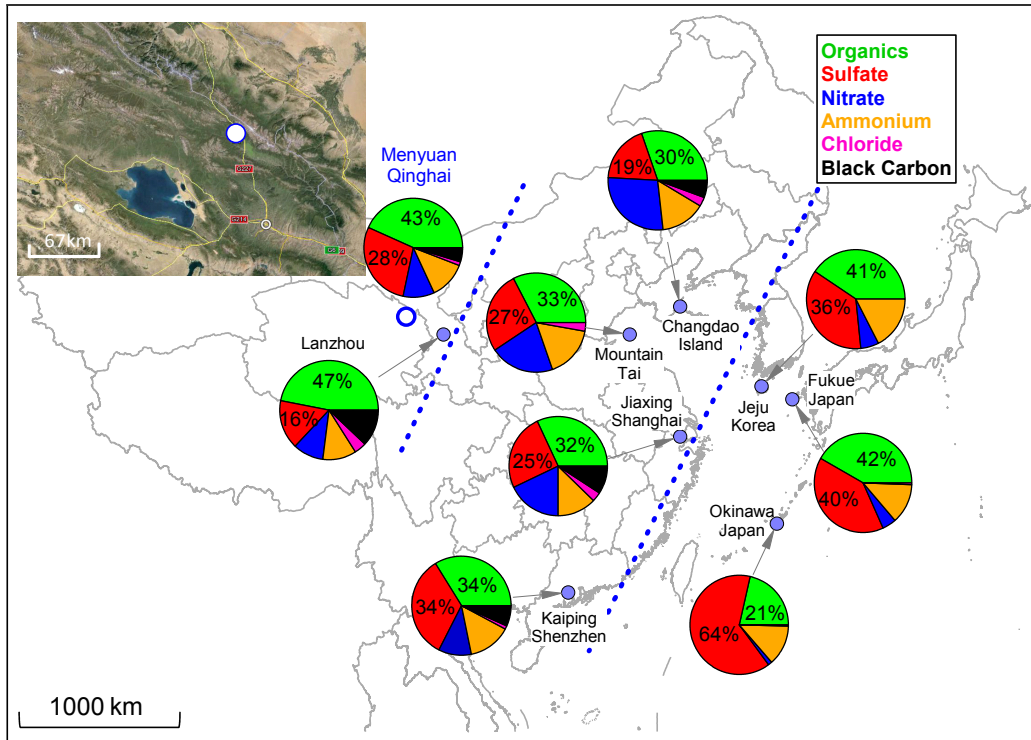
848 Figure 5. (a) Mass spectra and (b) time series of mass concentrations of BBOA and
849 OOA. The standard average mass spectra of BBOA and OOA in Ng et al. (2011) are
850 also shown for the comparison. The pie chart in (b) shows the average composition of
851 OA for the entire study.

852 Figure 6. Scatter plot of OOA versus SO₄ during BB and NBB periods. The data
853 points are color coded by BBOA concentrations. The pie chart shows the average
854 composition of OA with post-processed OOA ($= \text{OOA} - \text{SO}_4 \times [\text{OOA}/\text{SO}_4]_{\text{NBB}}$).

855 Figure 7. (a) The evolution of particle number size distributions; (b) average particle
856 number size distributions during NPE and non-NPE; (c,d) time series and diurnal
857 cycles of particle number concentrations for three different sizes. The log-normal
858 distribution fitting of each mode is shown in (b) as dash lines. The sunrise time was
859 around 7:00.

860 Figure 8. Diurnal evolution of particle size distributions, aerosol composition, gaseous
861 precursors, and the ratios of aerosol species to CO during (a) NPE and (b) non-NPE.
862 The sunrise time was approximately 7:00.

863 Figure 9. (a) Time series of OOA/PM₁, particle growth rates, and average chemical
864 composition during particle growth periods; (b) correlation of growth rate with
865 OOA/PM₁. The data points are color coded by the PM₁ mass concentration.



867

868

869

870

871

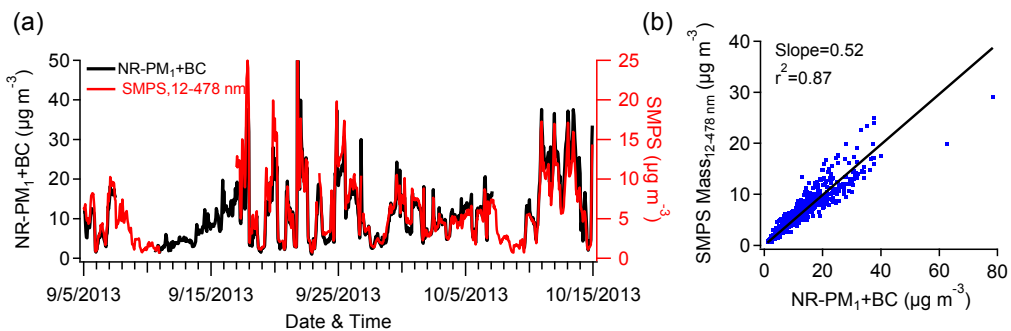
872

873

874

875

Figure 1. Map of the sampling site (Menyuan, Qinghai). Also shown is the chemical composition of submicron aerosols (NR-PM₁ + BC if it was available) measured at selected rural/remote sites in East Asia except Lanzhou, an urban site in northwest China. The two dotted blue lines are used to guide eyes for the three rural/remote regions from the west to the east. The detailed information of the sampling sites is presented in Table S1.



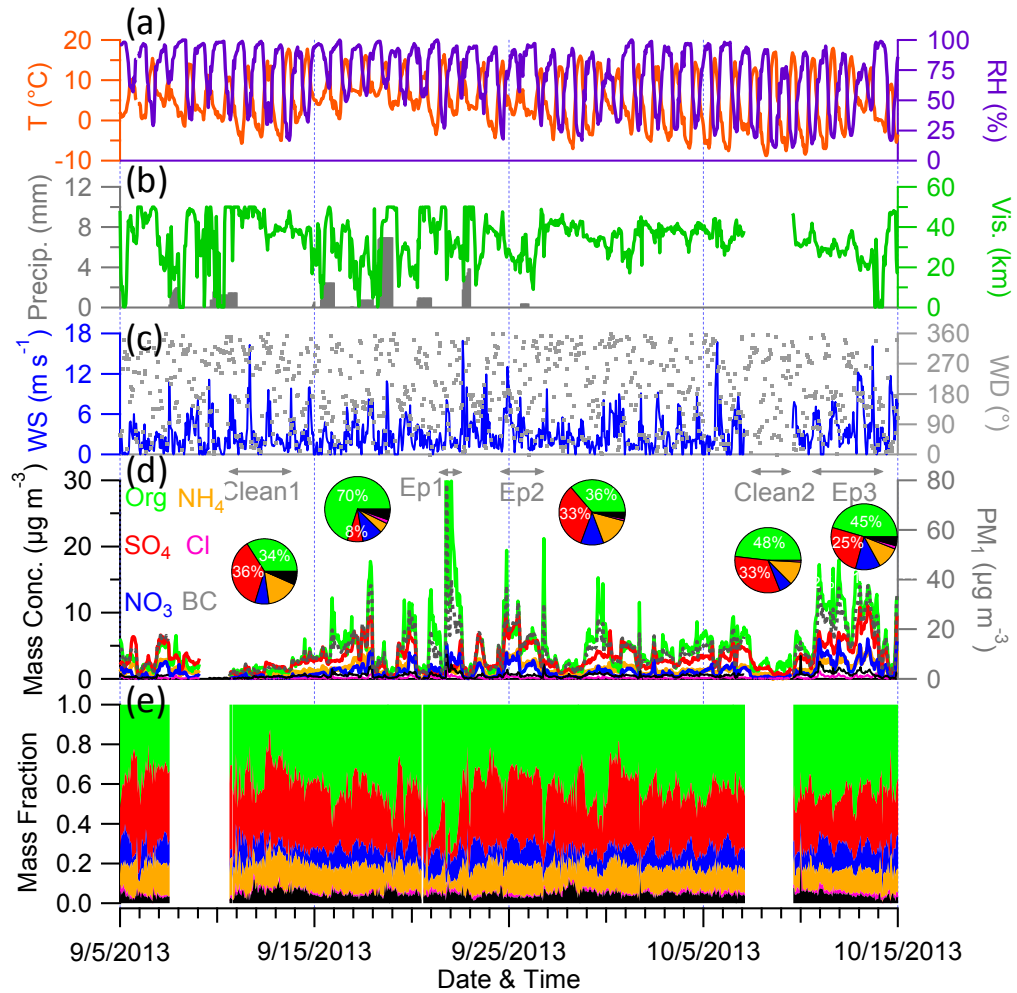
876

877

878

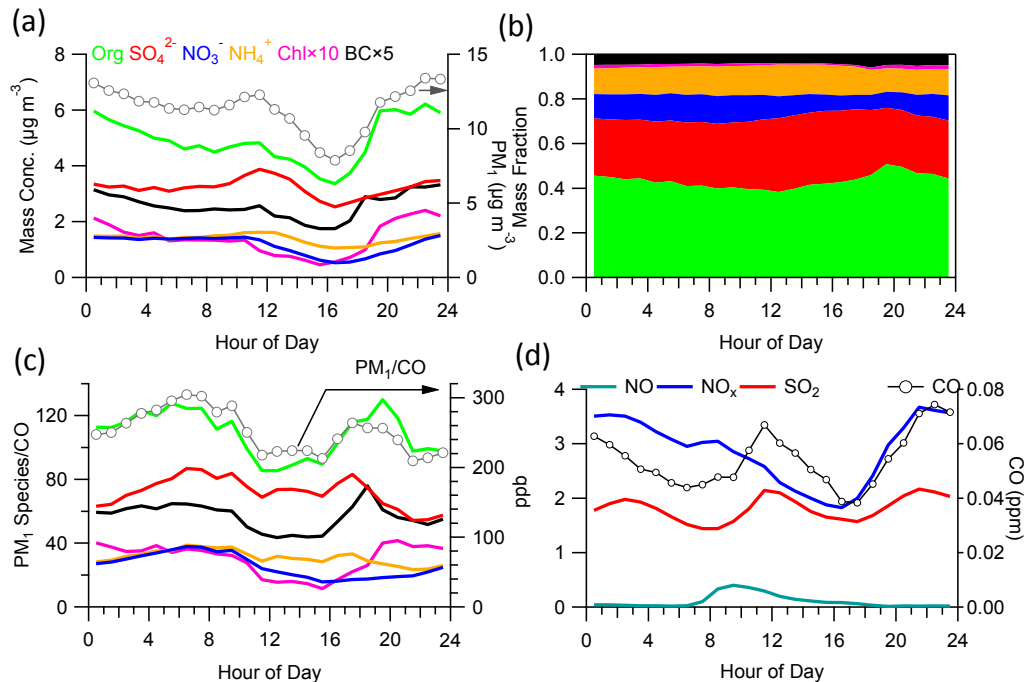
879

Figure 2. Comparison of the mass concentrations of PM₁ (NR-PM₁ +BC) measured by the ACSM and Aethalometer with that by the SMPS ($D_m = 12 - 478$ nm): (a) time series and (b) scatter plot.

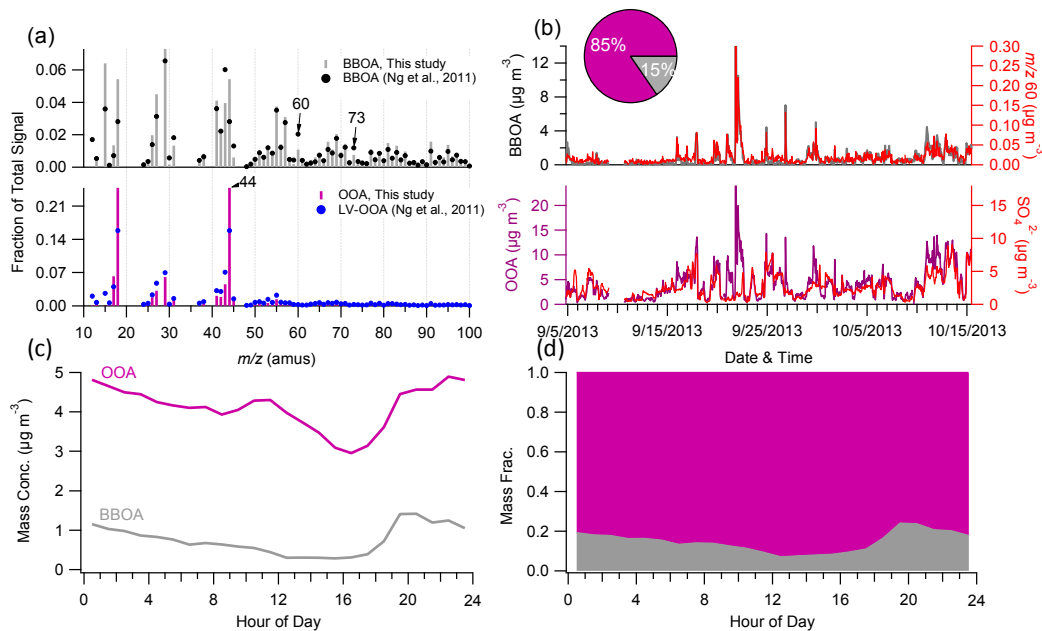


880

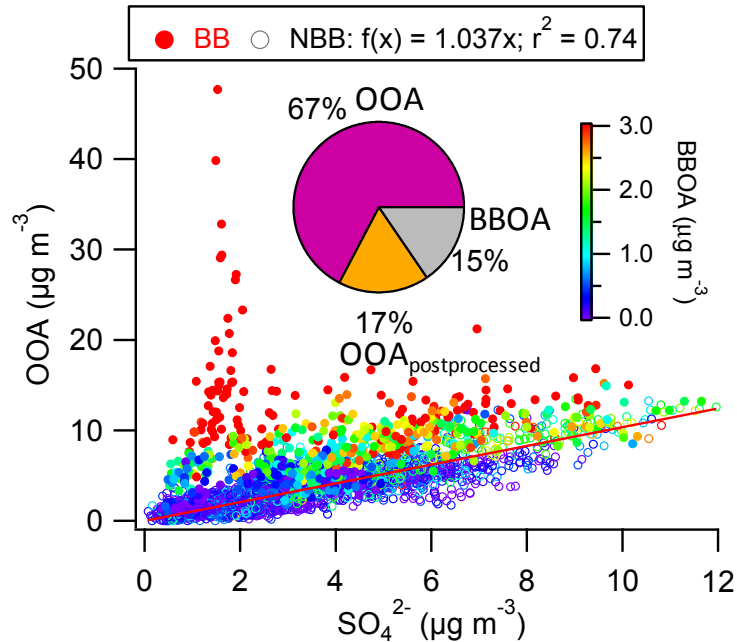
881 Figure 3. Time series of (a-c) meteorological variables including T (temperature), RH
 882 (relative humidity), Precip. (precipitation), WS (wind speed), WD (wind direction),
 883 and Vis (visibility), (d) mass concentrations and (e) mass fractions of PM₁ species .
 884 The pie charts show the average chemical composition of PM₁ for five episodes.



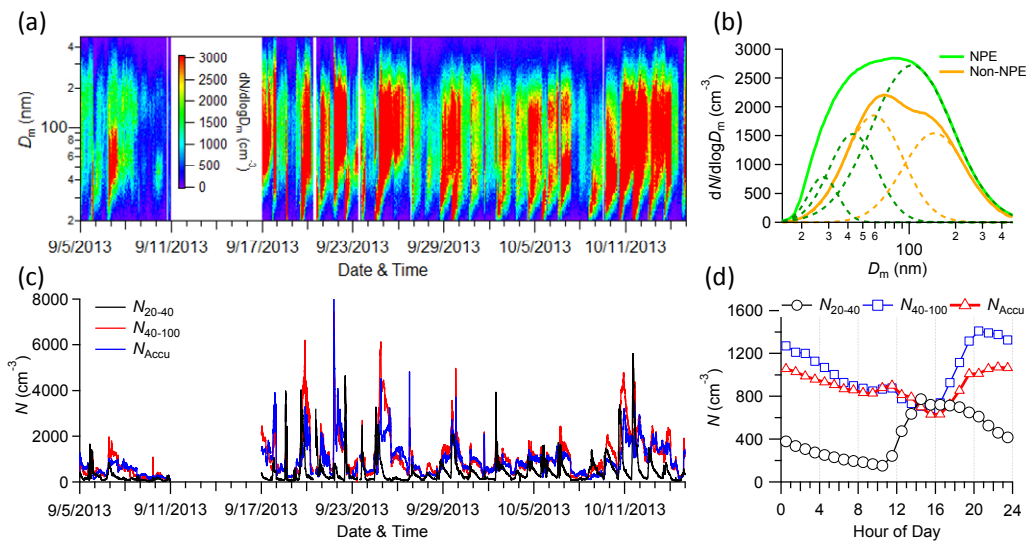
885
 886 Figure 4. Average diurnal cycles of (a) mass concentration; (b) mass fraction of PM₁
 887 species; (c) ratios of aerosol species to CO, and (d) gaseous species. The local sunrise
 888 and sunset was around 7:00 and 19:00, respectively.



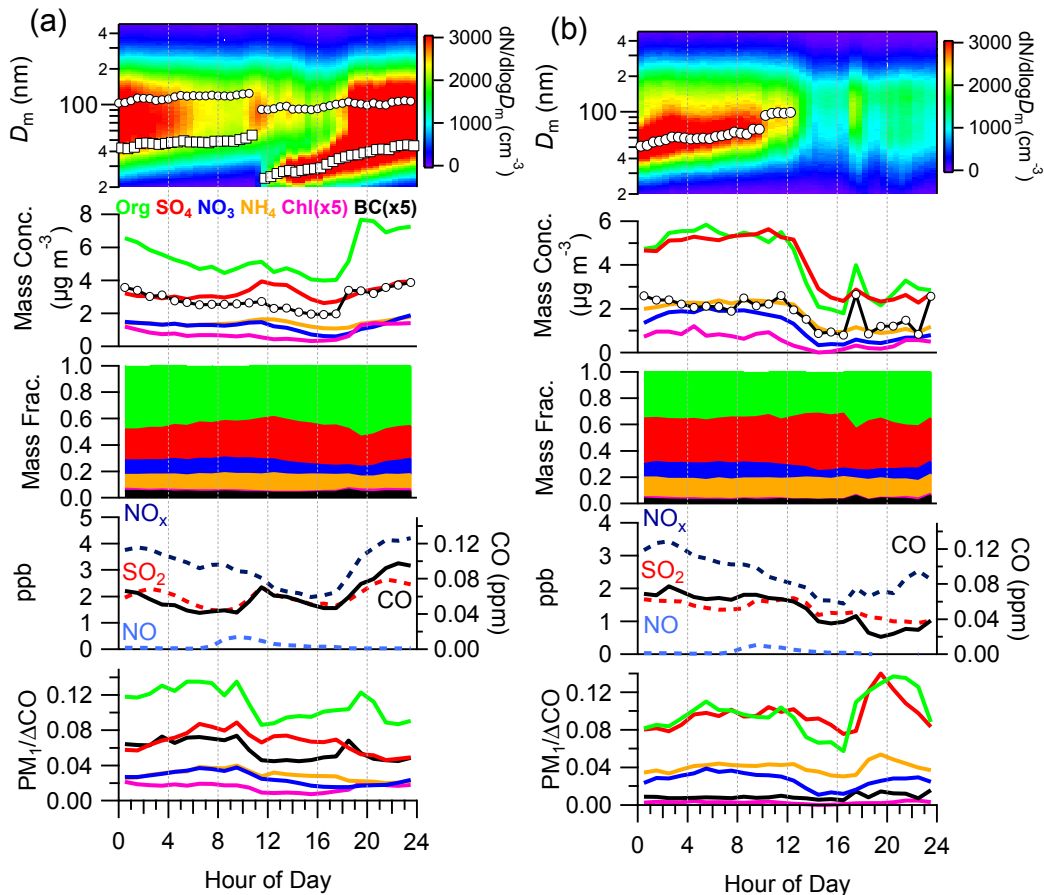
889
 890 Figure 5. (a) Mass spectra and (b) time series of mass concentrations of BBOA and
 891 OOA, (c) and (d) show the average diurnal cycles of BBOA and OOA. In addition,
 892 the standard average mass spectra of BBOA and OOA in Ng et al. (2011) are also
 893 shown in (a) for the comparison. The pie chart in (b) shows the average composition
 894 of OA for the entire study.



895
 896 Figure 6. Scatter plot of OOA versus SO_4 during BB and NBB periods. The data
 897 points are color coded by BBOA concentrations. The pie chart shows the average
 898 composition of OA with post-processed OOA ($= \text{OOA} - \text{SO}_4 \times [\text{OOA}/\text{SO}_4]_{\text{NBB}}$).

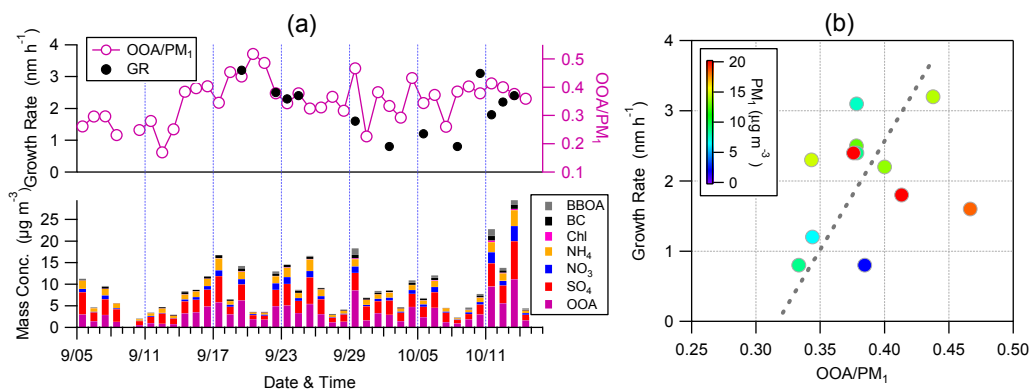


899
 900
 901 Figure 7. (a) The evolution of particle number size distributions; (b) average particle
 902 number size distributions during NPE and non-NPE; (c,d) time series and diurnal
 903 cycles of particle number concentrations for three different sizes. The log-normal
 904 distribution fitting of each mode is shown in (b) as dash lines. The sunrise time was
 905 around 7:00.



906

907 Figure 8. Diurnal evolution of particle size distributions, aerosol composition, gaseous
 908 precursors, and the ratios of aerosol species to CO during (a) NPE and (b) non-NPE.
 909 The sunrise time was approximately 7:00.



910

911 Figure 9. (a) Time series of OOA/PM₁, particle growth rates, and average chemical
 912 composition during particle growth periods; (b) correlation of growth rate with
 913 OOA/PM₁. The data points are color coded by the PM₁ mass concentration.